Received: 20 December 2020 | Revised: 27 January 2021 | Accepted: 2 February 2021

DOI: 10.1002/agt2.36

Aggregate WILEY Open Access

RESEARCH ARTICLE

Revisiting an ancient inorganic aggregation-induced emission system: An enlightenment to clusteroluminescence

Zheng Zhao[1,2,4] | **Zaiyu Wang**[1] | **Javad Tavakoli**[3] | **Guogang Shan**[1] | **Jianyu Zhang**[1] | **Chen Peng**[1] | **Yu Xiong**[4] | **Xuepeng Zhang**[1] | **Tsz Shing Cheung**[1] | **Youhong Tang**[5] | **Bolong Huang**[6] | **Zhaoxun Yu**[7] | **Jacky W. Y. Lam**[1] | **Ben Zhong Tang**[1,4,8]

[1] Department of Chemistry, Hong Kong Branch of Chinese National Engineering Research Center for Tissue Restoration and Reconstruction and Institute for Advanced Study, The Hong Kong University of Science and Technology, Clear Water Bay, Kowloon, Hong Kong SAR, China

[2] School of Chemistry and Chemical Engineering, Southeast University, Nanjing, China

[3] Centre for Health Technologies, School of Biomedical Engineering, University of Technology Sydney, Sydney, New South Wales, Australia

[4] HKUST Shenzhen Research Institute, Shenzhen, Guangdong, China

[5] College of Science and Engineering, Flinders University, Adelaide, South Australia, Australia

[6] Department of Applied Biology and Chemical Technology, The Hong Kong Polytechnic University, Hung Hom, Kowloon, Hong Kong SAR, China

[7] Micro-X Ltd, Tonsley, South Australia, Australia

[8] Guangdong-Hong Kong-Macao Joint Laboratory of Optoelectronic and Magnetic Functional MaterialsGuangdong-Hong Kong-Macao, China

Correspondence
Ben Zhong Tang, Department of Chemistry, Hong Kong Branch of Chinese National Engineering Research Center for Tissue Restoration and Reconstruction and Institute for Advanced Study, The Hong Kong University of Science and Technology, Clear Water Bay, Kowloon, Hong Kong SAR, China.
Email: tangbenz@ust.hk
Youhong Tang, College of Science and Engineering, Flinders University, Adelaide, South Australia, Australia.
Email: youhong.tang@flinders.edu.au
Bolong Huang, Department of Applied Biology and Chemical Technology, The Hong Kong Polytechnic University, Hung Hom, Kowloon, Hong Kong SAR, China.
Email: bolong.huang@polyu.edu.hk

Zheng Zhao, Zaiyu Wang, and Javad Tavakoli contributed equally to this work.

Funding information
National Natural Science Foundation of China, Grant/Award Numbers: 21788102, 52003228; Science and Technology Plan of Shenzhen, Grant/Award Number: JCYJ20180306174910791; Natural Science Foundation of Guangdong Province, Grant/Award Number: 2019B121205002; Research Grants Council of Hong Kong, Grant/Award Numbers: N_HKUT609/19, 16305518, A-HKUST605/16, C6009–17G; Innovation and Technology Commission, Grant/Award Numbers: ITC–CNERC14SC01, ITCPD/17–9

Abstract

Organic and inorganic clusteroluminescence have attracted great attention while the underlying mechanisms is still not well understood. Here, we employed a series of ancient inorganic complexes platinocyanides with aggregation-induced emission property to elucidate the mechanism of clusteroluminescence including how does the chromophore form and how does the solid structures influence the luminescence behaviors. The results indicate that the isolated platinocyanide cannot work as a chromophore to emit visible light, while their clusterization at aggregate state can trigger the d-orbitals coupling of the platinum atoms to facilitate the electron exchange and delocalization to form a new chromophore to emit visible light. Furthermore, the counter ions and H_2O ligands help to rigidify the three-dimensional network structure of the platinocyanides to suppress the excited state nonradiative decay, resulting in the high quantum yield of up to 96%. This work fundamentally helps understanding both the organic and inorganic clusteroluminescence phenomenon.

KEYWORDS
aggregation-induced emission, clusteroluminescence, radioluminescence

1 | INTRODUCTION

During the course of human civilization, the role of materials is so significant that people have used a specific kind of material to name an era such as the stone age, iron age, bronze age, and even today's silicon age.[1,2] As the earliest materials utilized by human, the remolding and research of stone materials has a long history, with luminescent stone as one of them.[3] There are many ancient reports or descriptions about luminescent stones, such as the western "Bolognian Stone" and eastern "Luminous Pearl" etc.[4–7] Among these luminescent stones, a representative one that has been systematically investigated is fluorite that was reported by Edward D. Clarke and coworkers in 1819, although no explanation for its luminescent phenomenon was provided at that time.[4] Until one century later, Haberlandt et al. pointed out that the blue emission of fluorite came from the inorganic compound europium(II) chloride contained in it.[7] Based on those pioneering discoveries and continuous exploration, inorganic luminescent materials experienced a burgeoning development and have greatly promoted human civilization and technology advancement.[8–13] Although orbital theory and semiconductor theory have been commonly utilized to explain the inorganic luminescent systems, the detailed photophysical process of these inorganic luminescent materials still need to be further explored, as it commonly suffers the influence of mixture, impurities, and quantum effect.[9]] Furthermore, some interesting phenomenons such as the aggregation-induced emission (AIE, vide infra) property of inorganic clusters is difficult to explain by the traditional photophysical models.[11–17]

On the other hand, the development of organic chemistry has initiated the era of organic materials. In comparison with inorganic luminescent materials, organic luminescent materials not only have accurate molecular structures but also are much richer in amount, variety, and chemical modification, which enables systematical structure–property relationship study. As a result, the theoretical framework of organic photophysics is well established based on the deep research of molecular photophysics, which in many cases can effectively guide the molecular design of luminescent molecules and explain the emerging photophysical phenomenons.[18–21] However, in general, these molecular photophysics models mainly follow the philosophy of reductionism, which claims that all objects and properties are reducible to a single entity such as the molecules.[22] Although the macroscopic property of a substance is consistent with the molecules that they are composed of in many cases, there is also some inconsistency between the microscopic molecule and the macroscopic substance. For instance, some fluorescent molecules with planar structure show bright emission in their isolated state but quenched emission when they form aggregates.[23] More interestingly, in a few cases, there is also some molecular system that show nonemission in their isolated state but bright emission in their aggregation state, which has been coined as AIE in 2001.[23] It is obvious that AIE case is not suitable to be simply considered by traditional molecular photophysics models that are based on a single molecule, since these models are proposed with main focus on molecules rather than aggregates.[22] In general, although several groups have observed the AIE phenomenon, these cases were mainly treated as abnormal luminescent systems without a good understanding and did not attract too much attention before 2001.[24–27]

An even more interesting AIE phenomenon is clusteroluminescence. Clusteroluminescence is another exception that cannot be simply explained by traditional molecular photophysics, as some of them even do not contain any typical chromophore such as phenyl ring.[28–32] Typical clusteroluminescent molecules such as natural cellulose, polysaccharide, polypeptide, proteins, and some artificial polymers generally are nonconjugated and only comprise some sp3 carbon-connected heteroatoms or amide groups.[33–36] In spite of their nonconjugated molecular structures, they show bright visible emission once they are clustered to form aggregates. By comparing these organic cellulose or polysaccharide with the previously mentioned inorganic luminescent system like europium(II) chloride, it is obvious they show some similarities: (1) they all lack typical chromophore defined by traditional molecular photophysics; (2) they all exhibit AIE characteristic which are not emissive in dilute solution but brightly emissive in visible region when clustered or aggregated; (3) their luminescence properties mostly correlate closely with their aggregate characteristics such as morphology and alignment. Why the clusterization of these nonconjugated systems emits visible light? What kind of chromophore they have formed during the clusterization? How their aggregation influences their photophysical properties? These questions are not well understood while the implication of which is far reaching. Thereby, elucidation of the underlying mechanism of this clusterization-triggered emission fundamentally is significant for both organic and inorganic clusteroluminescence phenomenon and practically also benefits the development of advanced luminescent materials.

In 1853, When George Stokes studied the luminescence of $BaPt(CN)_4$, he observed an interesting phenomenon as he described in one of his publications "It is only in the solid state that the platinocyanides are sensitive (means emissive), their solutions are like mere water (means nonemissive)," which possibly is the earliest description of AIE phenomenon although the term AIE had not been proposed at that time.[37] However, the author did not give further explanation for the special luminescence phenomenon of these platinocyanides at that time due to the limitation in understanding the luminescence phenomenon. Other groups studied the optical properties of platinocyanides or their analogs later.[38–41]] However, under the guidance of the traditional scientific paradigm of reductionism, these research generally still focus on the properties in solution state, scarcely considering the influence of packing mode, aggregate morphology, and counter ions on the luminescence properties. Consequently, the fundamental questions about the AIE behavior of the platinocyanides were still not well elucidated. Because the platinocyanide system maybe the firstly reported inorganic AIE system without typical π-conjugated chromophore, elucidation of the underlying mechanism including how does the chromophore form and how does the aggregate influence the luminescence is quite significant in understanding both the inorganic and organic clusteroluminescence. In consideration of these, we revisited this ancient AIE system and

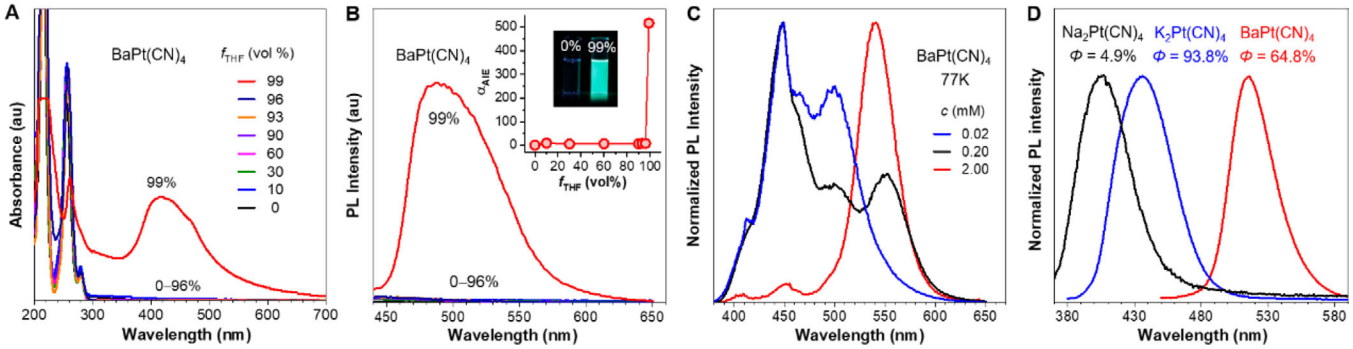

FIGURE 1 (A) Absorption and (B) Photoluminescence (PL) spectra of $BaPt(CN)_4$ in H_2O/THF mixtures (20 μM) with different THF fractions (f_{THF}), excitation wavelength (λ_{ex}): 365 nm. Inset: The plot of the emission maximum intensity versus the composition of the aqueous mixture of $BaPt(CN)_4$ with different f_{THF}. $\alpha_{AIE} = I/I_0$; I_0 is the emission maximum intensity in water solution. Luminescence photographs of $BaPt(CN)_4$ in water solution and in f_{THF} = 99% mixture taken under 365 nm UV irradiation. (C) PL spectra of frozen water solution of $BaPt(CN)_4$ at 77 K with different concentrations. (D) PL spectra and quantum yields of the crystals of $BaPt(CN)_4{\cdot}4H_2O$, $K_2Pt(CN)_4{\cdot}3H_2O$, and $Na_2Pt(CN)_4{\cdot}3H_2O$

systematically investigated the luminescence properties of both solution and aggregation state. In particular, we studied the influence of solid-state intermolecular interactions on the luminescence properties of these platinocyanides. The results indicate that (1) the emission of platinocyanide aggregates originate from the metal complex clusters formed in aggregates; (2) the resulted three-dimensional net framework after aggregation can effectively restrict the nonradiative decay and thus enhance the luminescence quantum yield (QY) to almost 100%; (3) the counter ions and water molecules take part in the formation of the three-dimensional net framework and contribute greatly to the molecular rigidification and the corresponding high luminescence QY. Based on these experimental data, we concluded that the enhanced atom–atom/group–group interactions and the rigidification effect after clusterization contribute greatly to the clusteroluminescence phenomenon. We hope this mechanistic understanding can trigger new advancement in both inorganic and organic clusteroluminescence.

2 | RESULTS AND DISCUSSION

The platinocyanides are obtained from commercial source with three times of recrystallization before the experiment. The UV-vis absorption and PL properties of the solution and aggregates of $BaPt(CN)_4$ were firstly investigated. As shown in Figure S1 and Figure 1, the water solution of $BaPt(CN)_4$ exhibits sharp absorption peaks in a very short wavelength region of 200−300 nm, which are unaffected by the concentration change in a range of 4−200 μM (Figure S1). However, on continuously adding poor solvent tetrahydrofuran (THF) into the water solution of $BaPt(CN)_4$ until the THF fraction (f_{THF}) approaches 99%, a new absorption band at around 420 nm appeared (Figure 1). The absorption peaks at around 200−300 nm are assigned to the absorption of $Pt(CN)_4^{2-}$, while the absorption band at around 420 nm could be ascribed to the formation of aggregates. The aggregates formation was further confirmed by dynamic light-scattering measurement (Figure S2). The PL spectra is well consistent with the absorption spectra, which showed no signal in a range of f_{THF} = 0−96%, but very bright green emission when f_{THF} = 99%. Therefore, $BaPt(CN)_4$ exhibits typical AIE characteristic (Figure 1B). Because the isolated $Pt(CN)_4^{2-}$ species in dilute solution just show much shorter absorption peaks in UV region and is nonemissive, and the aggregates show a redshifted absorption in visible region and show bright visible emission, we thus speculated that the aggregation might have generated new chromophores, which are responsible for the visible emission of $BaPt(CN)_4$ aggregates. To further understand the chromophore formation, we investigated the PL spectra of the aqueous solution of $BaPt(CN)_4$ at 77 K with different concentrations. Interestingly, although the absorption of aqueous $BaPt(CN)_4$ is unaffected by concentration at room temperature (299 K), the PL spectra changes with concentrations at 77 K. As shown in Figure 1C, at a concentration of 0.02 mM, the aqueous $BaPt(CN)_4$ exhibited two main emission peaks at 449 and 499 nm and two small shoulder peaks at 412 and 465 nm. This suggests that the low temperature triggered the formation of clusters/aggregates in dilute water solution of $BaPt(CN)_4$. This is easy to understand since the crystallization of water at 77 K would exclude the homogeneous distribution of solute molecules, leading to the clusterization of solute molecules.[42,43] At a concentration of 0.2 mM, the peak intensity at 499 nm showed a decrease, followed by a new peak emerging at around 550 nm, possibly because of the formation of larger clusters with stronger intermolecular interactions.[38] Further increasing the concentration to 2 mM causes an intense decrease of the shorter emission peak but obvious enhancement of the longer emission peak. Therefore, we can conclude that at low temperature, clusters form whose size and intermolecular interactions are varied with the increase of the concentration. Higher concentration may facilitate the formation of larger clusters with strong intermolecular interactions leading to the redshift of the emission wavelength. Besides $BaPt(CN)_4$, we also investigated the optical properties of other platinocyanides with different counter ions such as potassium and sodium ions (Figures S3 and S4). All of these platinocyanides are AIE-active, and with the counter ions changing from sodium to potassium and further to barium, the emission colors of their aggregates keep redshifting from violet to blue and to green, suggesting that the counter ions may influence the packing or alignment of the platinocyanide aggregates.

To further understand the influence of counter ions on the photophysical properties of the platinocyanides, we

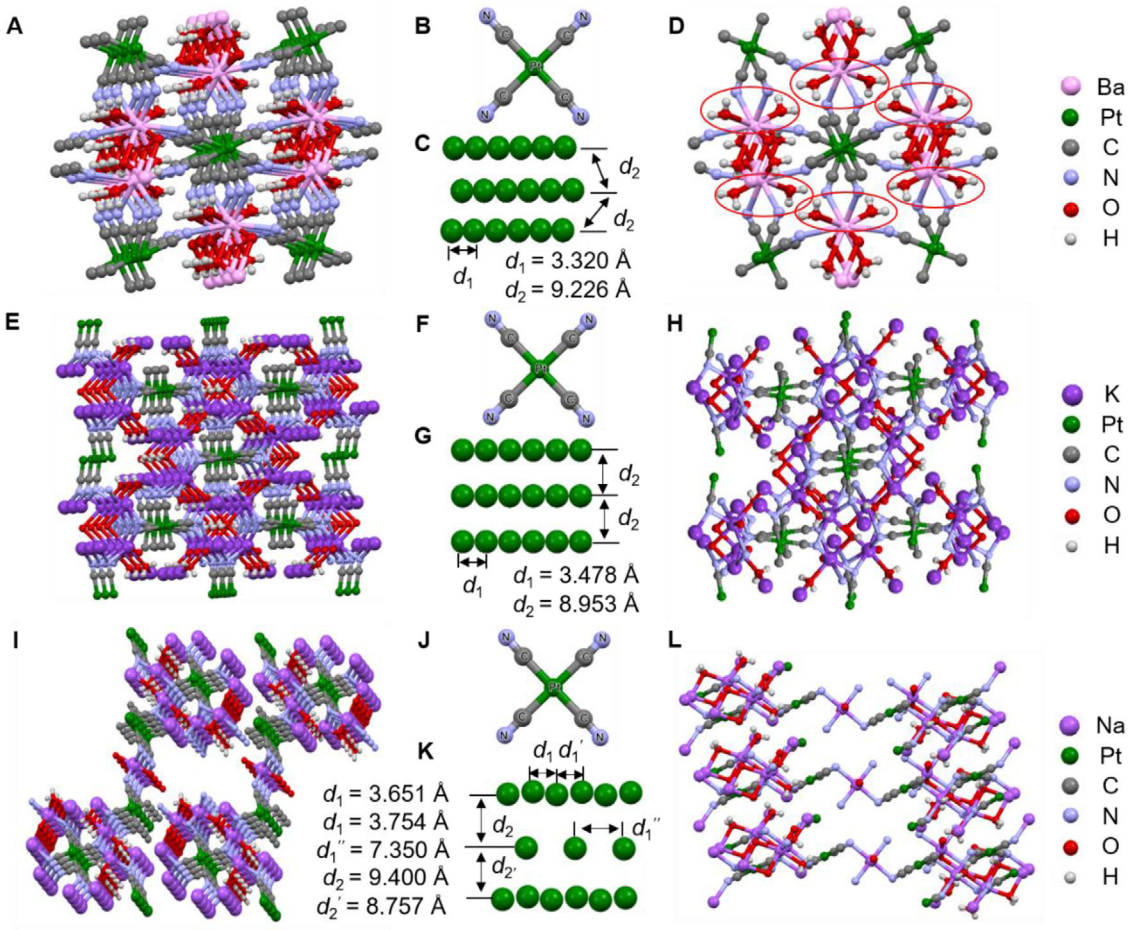

FIGURE 2 (A, E, I) Molecular packing arrangements in the crystals of $BaPt(CN)_4{\cdot}4H_2O$, $K_2Pt(CN)_4{\cdot}3H_2O$, and $Na_2Pt(CN)_4{\cdot}3H_2O$. (B, F, J) Molecular structures of $Pt(CN)_4^{2-}$ extracted from the packing structures of $BaPt(CN)_4{\cdot}4H_2O$, $K_2Pt(CN)_4{\cdot}3H_2O$, and $Na_2Pt(CN)_4{\cdot}3H_2O$. (C, G, K) Intermolecular Pt–Pt distances in the single crystals of $BaPt(CN)_4{\cdot}4H_2O$, $K_2Pt(CN)_4{\cdot}3H_2O$, and $Na_2Pt(CN)_4{\cdot}3H_2O$. (D, H, L) Intermolecular coordination interactions in the crystals of $BaPt(CN)_4{\cdot}4H_2O$, $K_2Pt(CN)_4{\cdot}3H_2O$, and $Na_2Pt(CN)_4{\cdot}3H_2O$

studied their absorption and emission properties in the solid state. As shown in Figure S5, the absorption spectrum of the crystals of $BaPt(CN)_4{\cdot}4H_2O$, $K_2Pt(CN)_4{\cdot}3H2O$, and $Na_2Pt(CN)_4{\cdot}3H_2O$ were similar, with some fine absorption peaks in the shorter wavelength region and a broad absorption band in the longer wavelength region. The peaks in the shorter wavelength region are identical with the absorption peaks of $Pt(CN)_4^{2-}$ in dilute solutions, while the continuously shifting absorption bands in the longer wavelength region obviously indicate that new chromophores with varied intermolecular interactions were formed in the solid state.[44] Excitation spectra of crystal and aggregates show excitation peaks with much longer wavelength than the absorption peaks of $Pt(CN)_4^{2-}$ in solution state, which also supports the formation of new chromophores in aggregates or solid state (Figure S6). The PL spectra of the crystals of $Na_2Pt(CN)_4{\cdot}3H2O$, $K_2Pt(CN)_4{\cdot}3H_2O$, and $BaPt(CN)_4{\cdot}4H_2O$ show similar tendency as absorption spectra, exhibiting continuous redshifted emission wavelengths from $Na_2Pt(CN)_4{\cdot}3H_2O$ to $K_2Pt(CN)_4{\cdot}3H_2O$, and to $BaPt(CN)_4{\cdot}4H_2O$, with emission peaks at 407, 436, and 515 nm, respectively (Figure 1D). These results suggest that from $Na_2Pt(CN)_4{\cdot}3H_2O$ to $K_2Pt(CN)_4{\cdot}3H_2O$ and to $BaPt(CN)_4{\cdot}4H_2O$, the intermolecular interactions become stronger and stronger, which causes the redshift of the emission wavelength. Interestingly, besides the emission wavelength, the QY of these platinocyanides also show large difference. The QY of the solutions of the platinocyanides generally are too low to detect. In the solid state, the crystal of $K_2Pt(CN)_4{\cdot}3H_2O$ exhibit a QY as high as 93.8%, as a contrast, the crystal of $Na_2Pt(CN)_4{\cdot}3H_2O$ exhibit a QY of merely 4.9%, and the QY of $BaPt(CN)_4{\cdot}4H_2O$ (64.8%) locates in between $K_2Pt(CN)_4{\cdot}3H_2O$ and $Na_2Pt(CN)_4{\cdot}3H_2O$. The QY of the three platinocyanides suggests that besides the emission wavelength, the excited state radiative decay and PL intensity in the solid state would also be influenced by the counter ions.

To understand the luminescence behaviors of these platinocyanides and elucidate the relationship among the counter ions, molecular alignment, and the photophysical properties, we investigated the single-crystal structures of these platinocyanides.[45–47] As shown in Figure 2, the molecular structure of the $Pt(CN)_4^{2-}$ is planar square, which is unaffected by the crystal alignment. However, in the crystals, the Pt centers of $Pt(CN)_4^{2-}$ in the adjacent layers interact with each other and form some interconnected columnar channel that benefits the charge transfer and energy splitting of the metal d orbitals, resulting in the bandgap decrease to visible region.[48] Therefore, it is reasonable to speculate that these columnar aligned $Pt(CN)_4^{2-}$ works as a chromophore and is responsible for the visible emission of the platinocyanides. Furthermore, the Pt–Pt distances of

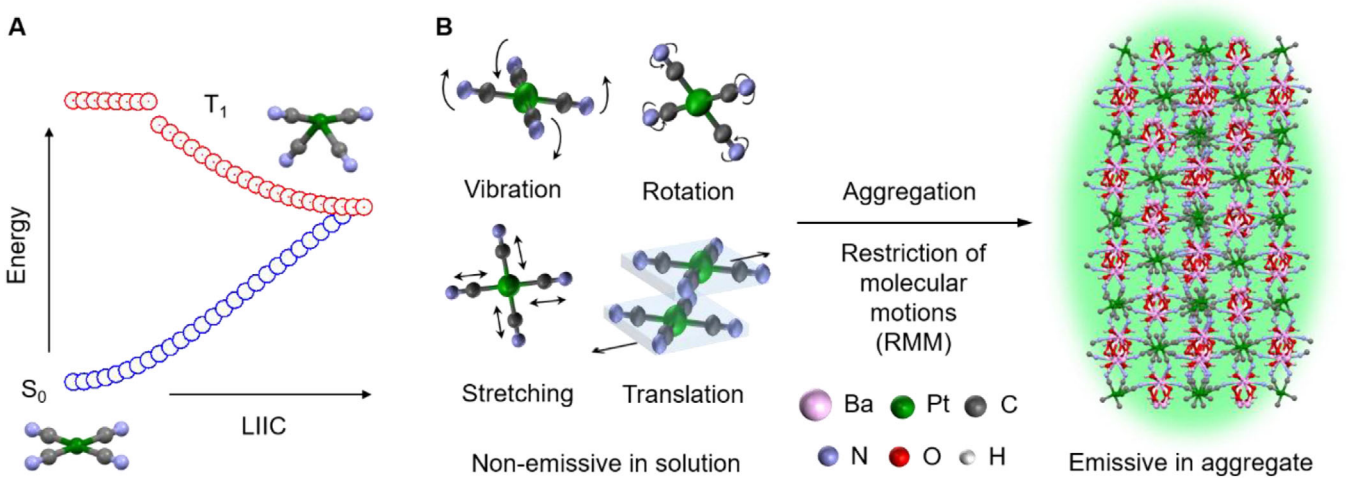

FIGURE 3 (A) Calculated linearly interpolated internal coordinate (LIIC) pathway and minimal energy conical intersection (MECI) between the optimized S_0 and T_1 geometries of isolated $Pt(CN)_4^{2-}$. (B) Mechanistic illustration of (left) molecular motions of $Pt(CN)_4^{2-}$ solution and (right) restriction of molecular motions (RMM) in $BaPt(CN)_4{\cdot}4H_2O$ crystal

$Na_2Pt(CN)_4{\cdot}3H_2O$ (3.651 and 3.754 Å), $K_2Pt(CN)_4{\cdot}3H_2O$ (3.478 Å), and $BaPt(CN)_4{\cdot}4H_2O$ (3.320 Å) gradually decrease, which exhibits a positive response to the gradually redshifted absorption and emission wavelengths of these platinocyanides, suggesting shorter Pt–Pt distance leads to narrower bandgap. It is worthy to note that a linear correlation between emission energies and d^{-3} (d: Pt–Pt distance) of these platinocyanides is observed (Figure S7), which actually has been explained from viewpoints of the electrostatic coupling of the transition dipole moments and orbital overlapping, and delocalization of the excited electron previously.[48–50] The intercolumn distances generally are too large to influence the electronic properties of these platinocyanides (Figure 2). On the other hand, due to different interconnections between alkali metal ions and $Pt(CN)_4^{2-}$ as well as the coordination interactions with H_2O molecules, the three-dimensional network structures of these platinocyanides also show large difference (Figure 2D,H,L). In the crystal of $BaPt(CN)_4{\cdot}4H_2O$, the four CN groups of $Pt(CN)_4^{2-}$ are locked by Ba^{2+} to form the relatively rigid 3D network structure, which helps reduce the nonradiative decay promoted by excited state molecular motion. Four water molecules participate in the construction of the 3D network structure, with two of the H_2O are totally locked and two are semi-locked (Figure 2D, highlighted by red circles). Similarly, the CN groups in the crystal of $K_2Pt(CN)_4{\cdot}3H_2O$ are locked by K^+ to form a more compact 3D network, in which three H_2O molecules take part in the coordination and all of them are totally locked in the network structure. The relative more compact 3D network of $K_2Pt(CN)_4{\cdot}3H_2O$ than $BaPt(CN)_4$ is consistent with their QY data, where more compact and rigid network structure gives much higher QY value. In comparison with $BaPt(CN)_4{\cdot}4H_2O$ and $K_2Pt(CN)_4{\cdot}3H_2O$, the packing of the 3D network of $Na_2Pt(CN)_4{\cdot}3H_2O$ is relatively loose, and the connections or bridge interactions between the layers are obviously less than $BaPt(CN)_4{\cdot}4H_2O$ and $K_2Pt(CN)_4{\cdot}3H_2O$, which also matches well with its much low QY of 4.9%. The loose packing of the crystal will cause more active excited state molecular motion to quench the emission according to the mechanism of AIE.[51]

Based on the crystal analysis and the photophysical properties of these platinocyanides, we proposed the possible working mechanism for this inorganic AIE system (Figure 3). Generally speaking, the single $Pt(CN)_4^{2-}$ with limited conjugation is unable to work as a chromophore to emit visible light, and the calculation results indicate that the active excited state molecular motion of $Pt(CN)_4^{2-}$ also facilitates the nonradiative decay and are unfavorable for luminescence (Figures 3A and S8). However, the aggregation/clusterization of $Pt(CN)_4^{2-}$ not only helps restrict the possible excited state molecular motions like rotation, vibration, stretching, and translation, but also enables the formation of electron delocalized metal complex channel to work as a chromophore to emit visible light. According to this mechanism, the low QY of $Na_2Pt(CN)_4{\cdot}3H_2O$ crystals could be well explained, since loose packing of the crystal structure of $Na_2Pt(CN)_4{\cdot}3H_2O$ is unable to effectively restrain the active excited molecular motion of $Pt(CN)_4^{2-}$, which thus quenches its emission. While for $BaPt(CN)_4{\cdot}4H_2O$ and $K_2Pt(CN)_4{\cdot}3H_2O$, the compact and rigid 3D network structure can restrain the excited state molecular motions effectively and thus suppress the nonradiative decay, affording the much higher QY. The chromophore-forming mechanism was also supported by density functional theory (DFT) calculation through comparing the calculated results of the isolated state and frozen state of $Pt(CN)_4^{2-}$ based on the crystal structure of $BaPt(CN)_4$ (Figures S9 and S10). Notably, the active bonding and antibonding near the Fermi level in the frozen aqueous solution of $BaPt(CN)_4$ demonstrate that the electron mainly distributes around Pt sites within the $Pt(CN)_4^{2-}$ units. (Figure S9A). In particular, we can observe the long-range d orbital couplings between adjacent $Pt(CN)_4^{2-}$ units, which should be the dominant factor in promoting the electron transfer and delocalization (Figure S9B). Projected partial density of states (PDOS) results further confirmed the Pt-5d orbitals of the frozen lattice structure of $BaPt(CN)_4$ are located at the highest position to the Fermi level, which are the effective electron delocalized center for luminescence (Figure S9C). As a comparison, in the solution state, the dominant peak of Pt-5d orbitals in the freely migrating $Pt(CN)_4^{2-}$ units shift to

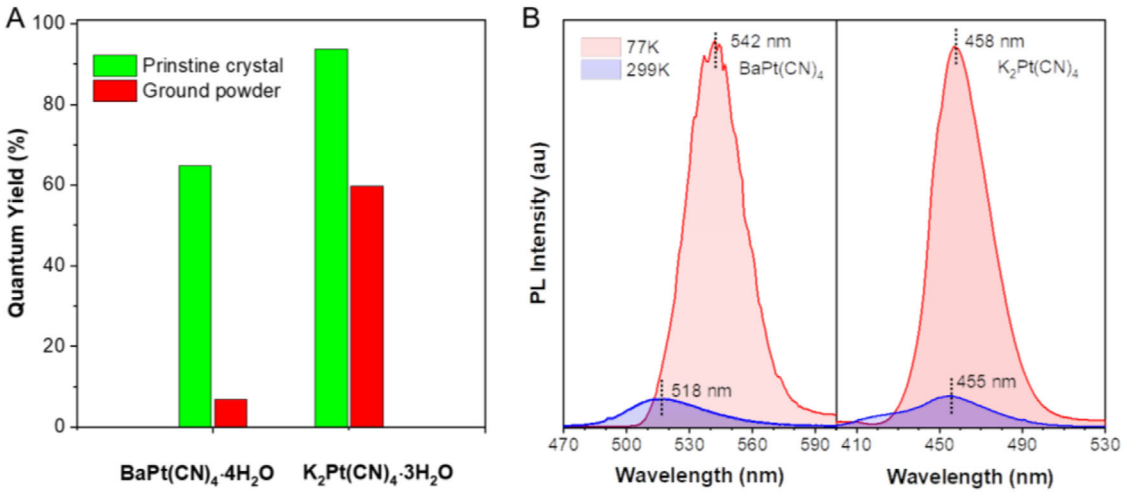

FIGURE 4 (A) Quantum yields of pristine crystal and ground powder of $BaPt(CN)_4{\cdot}4H_2O$ and $K_2Pt(CN)_4{\cdot}3H_2O$ measured by an integrating sphere; λ_{ex}: 365 nm. (B) PL spectra of crystals of (left) $BaPt(CN)_4{\cdot}4H_2O$ and (right) $K_2Pt(CN)_4{\cdot}3H_2O$ at 77 and 299 K; λ_{ex}: 365 nm

a deeper position at −3.5 eV while s and p orbitals of CN^- dominate the valence band maximum (VBM) (Figure S9D). The calculated dielectric function relative to excitation energy shows that both ε1 (real part) and ε2 (imaginary part) increase with the increase in the aggregation layer, which reveals the improved response of the low energy band to the external excitation with the enhancement of the aggregation level of $Pt(CN)_4^{2-}$ (Figure S9E). More importantly, the increase of the aggregation level of $Pt(CN)_4^{2-}$ leads to the decrease of the excitation energy from VB to CB, which benefits the formation of the chromophore in the visible range (Figure S9F). Time-dependent DFT (TDDFT) calculation gives the relative oscillator strengths of the different aggregates of $Pt(CN)_4^{2-}$, which indicates the transition probabilities of an electron on each excited state (Figure S10). For the freely migrating $Pt(CN)_4^{2-}$ in solution state, the electronic levels locate in a large energy range up to 3.20 eV, in which most of the electronic levels show very low electron transition probabilities (<.1), resulting in the low possibility of electron excitation. Meanwhile, as $Pt(CN)_4^{2-}$ units start to aggregate, the energy ranges of electronic states have been reduced to less than 1.0 and 0.8 eV, respectively, supporting the significantly improved electron excitation efficiency from VBM, which is well consistent with the emission wavelength redshift of the aggregates relative to isolated $Pt(CN)_4^{2-}$ (Figure S9G). Therefore, theoretical calculations match well with the experimental results, which supports that the long-range d–d coupling of $Pt(CN)_4^{2-}$ within the $BaPt(CN)_4$ aggregates is responsible for the formation of the chromophore. A more detailed sketch diagram of the whole AIE picture and chromophore-formation mechanism is given in Figure S11.

Apart from the chromophore-formation mechanism, we proposed that the luminescence efficiency depends on the molecular structure rigidity, which intrinsically related to the extent of excited state molecular motion. To demonstrate this hypothesis, the influence of the excited state molecular motion on the luminescence efficiency was investigated. Taking the crystal of $BaPt(CN)_4{\cdot}4H_2O$ and $K_2Pt(CN)_4{\cdot}3H_2O$ as an example, the QY of their ground powder generally are lower than their crystal as shown in Figure 4A. This is because the rigid 3D network structure of $BaPt(CN)_4{\cdot}4H_2O$ and $K_2Pt(CN)_4{\cdot}3H_2O$ was destructed, causing the suppression to excited state molecular motion weakened and thus decreasing the QY. Temperature is another factor that influences the excited state molecular motion, as shown in Figure 4B, lowering the temperature from room temperature to 77 K, both the emission intensity of the crystals of $BaPt(CN)_4{\cdot}4H_2O$ and $K_2Pt(CN)_4{\cdot}3H_2O$ show a large extent of enhancement, followed by a redshift of the emission wavelength. The luminescence enhancement obviously originates from the effectively restricted molecular motion, while the emission wavelength redshift could be ascribed to the further proximation of the Pt metal centers due to the shrink of the crystal at 77 K. Additionally, we have also evaluated the influence of temperature increase on the luminescence behavior of the crystals of $BaPt(CN)_4{\cdot}4H_2O$ and $K_2Pt(CN)_4{\cdot}3H_2O$. As shown in Figure 5, with the temperature increasing from 26°C to 160°C under N_2 protection, the luminescence of $BaPt(CN)_4{\cdot}4H_2O$ becomes yellow at around 80°C firstly and then becomes blue at around 140°C, which is accompanied by a weaken luminescence. Figure 5B shows the corresponding luminescence wavelength change of $BaPt(CN)_4{\cdot}4H_2O$ crystal upon temperature increase, which shows a redshift firstly and then a blueshift. Thermal gravimetric analysis (TGA) and differential scanning calorimetry (DSC) analysis indicate that the luminescence color change is accompanied by a loss of H_2O during the heating process. The emission color change from green to yellow at around 80°C is assigned to the loss of two semi-locked H_2O as mentioned previously in the crystal part, while the emission color change from yellow to blue at around 140°C is assigned to the loss of another two H_2O. Since the H_2O molecules act as ligand to take part in the construction of the 3D network structure of $BaPt(CN)_4{\cdot}4H_2O$ crystals, the loss of H_2O molecules thus would destroy the compact 3D network structure and reduce the excited state molecular motion suppression capability of the 3D network structure, causing decrease of the luminescence intensity. Similarly, $K_2Pt(CN)_4{\cdot}3H_2O$ also shows an emission color change during the heating process followed by the loss of H_2O molecules through the TGA and DSC analyses. The gradually weakened emission upon heating could also be ascribed to the destruction of the

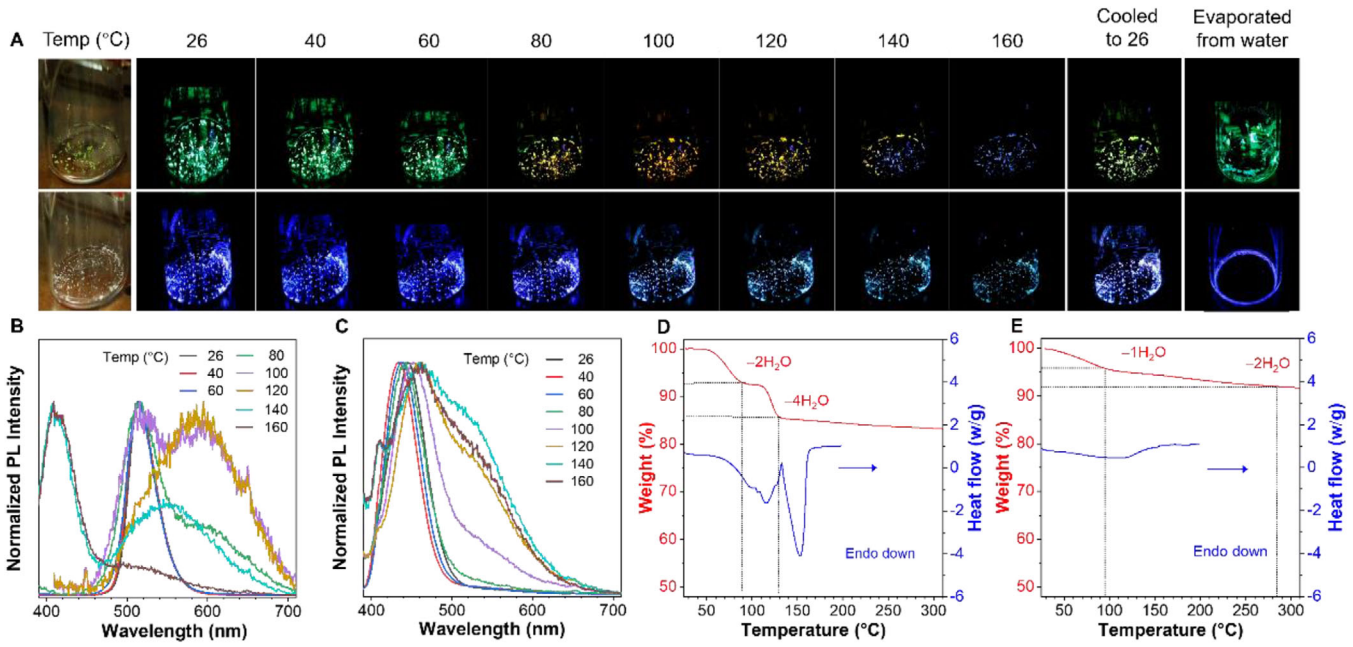

FIGURE 5 (A) Photos of crystals of $BaPt(CN)_4{\cdot}4H_2O$ and $K_2Pt(CN)_4{\cdot}3H_2O$ taken under irradiation of a UV light (365 nm) at different temperatures; the last two photos were taken after the sample was cooled to 26°C and its water solution was naturally evaporated. (B and C) Normalized PL spectra of crystals of (B) $BaPt(CN)_4{\cdot}4H_2O$ and (C) $K_2Pt(CN)_4{\cdot}3H_2O$ measured at different temperatures. (D and E) Thermal gravimetric analysis and differential scanning calorimetry data of crystals (D) $BaPt(CN)_4{\cdot}4H_2O$ and (E) $K_2Pt(CN)_4{\cdot}3H_2O$; heating rate: 10°C/min

3D network structure of $K_2Pt(CN)_4{\cdot}3H_2O$, which accelerates the excited state molecular motion. It is worthy to note for both $BaPt(CN)_4{\cdot}4H_2O$ and $K_2Pt(CN)_4{\cdot}3H_2O$, their luminescence properties including emission color and intensity can only partially recover relative to the initial state when removing the heating source and cooling to room temperature. For example, $BaPt(CN)_4{\cdot}4H_2O$ exhibits yellow emission while $K_2Pt(CN)_4{\cdot}3H_2O$ exhibits kind of bluish-white emission after cooling to room temperature, which actually is the mixture of blue light and yellow light, these phenomena suggest that only partial H_2O ligands could be recoordinated during the cooling, which may change the charge transfer and packing states of the crystals and thus change their emission. When redissolving the heated samples in water and undergoing evaporation, their luminescence properties can recover to the initial state due to the recrystallization. Therefore, these data further support that for these platinocyanides, the emission wavelength depends on the strength of the Pt–Pt interaction, while the rigid 3D network played an essential role in affording the high luminescence efficiency. The metal counter ions and H_2O take part in the construction of the 3D network and thus indirectly influence the luminescence performance.

It is worthy to note that those organic nonconjugated luminescent systems such as cellulose, polysaccharide, and polypeptide owned no typical chromophore-like aromatics or conjugated unsaturated bonds but exhibited similar clusteroluminescence phenomenon as these platinocyanides.[28] We can thus put them together to consider the general picture for the chromophore-forming process and the reason of emission enhancement with the clusterization process. By summarizing their similarities, we concluded that the enhanced atom–atom/group–group interactions can facilitate the electron communication and delocalization within the closely linked atoms or groups to form the chromophore to emit visible light and the rigidification effect after clusterization contributes greatly to the strong emission of the clusters.

Since the heavy metal atoms generally have effective absorption to the radioactive rays, which implies these platinocyanides possibly could be excited by X-ray. We thus evaluated the radioluminescence (RL) property of these platinocyanides. As shown in Figure 6, both $BaPt(CN)_4$ and $K_2Pt(CN)_4$ could be excited by X-ray to emit green and blue luminescence, respectively, and the emission wavelengths are in accordance with that of their photoluminescence. RL intensity of both $BaPt(CN)_4$ and $K_2Pt(CN)_4$ shows a near-linear increase to the exerted voltages. However, $Na_2Pt(CN)_4$ does not show RL property. The RL property suggests that these platinocyanides potentially could be used for high penetration depth imaging, since X-ray as excitation source could penetrate most of the tissues.[52–54] As a demonstration, we put some powder of $BaPt(CN)_4$ into a hole of a sheep bone. When irradiated on the top of the bone by UV lamp without directly irradiating the sample, the powders of $BaPt(CN)_4$ does not show any luminescence since the UV light cannot penetrate the dense sheep bone. Nevertheless, when using X-ray to irradiate the top of the bone, the $BaPt(CN)_4$ in the hole of bone could be successfully excited to emit green light. Therefore, comparing to the PL emitters, luminogens with RL does not suffer from the limitation of penetration depth of excitation light. The disadvantages of autofluorescence, poor signal-to-noise ratio, and poor tissue penetration depth that suffer by traditional PL emitters thus could be elegantly solved by RL luminogens. Furthermore, some advanced applications such as optogentics that utilize photo to control the activity of neuron cells also require luminogens with large penetration depth.[55] These advantages demonstrate the great potential of the RL luminogens in bioimaging, especially deep tissue imaging.

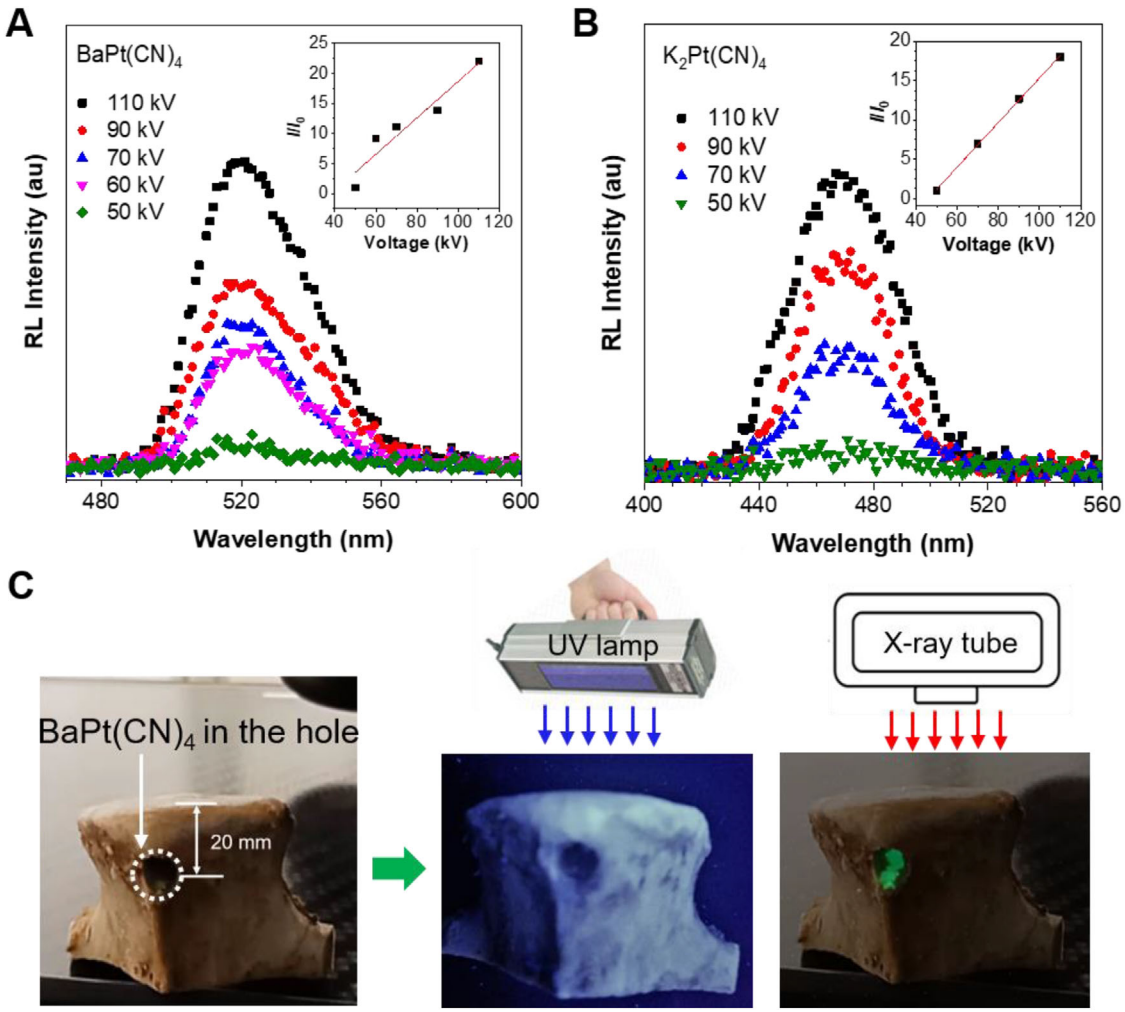

FIGURE 6 Radioluminescence spectra of the crystals of (A) $BaPt(CN)_4 \cdot 4H_2O$ and (B) $K_2Pt(CN)_4 \cdot 3H_2O$ at different radiation doses by a fiber optic spectrometer. Inset: The plot of radioluminescence intensity versus the applied voltages. (C) Photos of $BaPt(CN)_4 \cdot 4H_2O$ powders hidden in a hole of a sheep bone taken under excitation by a UV lamp (λ_{ex}: 365 nm) and X-ray tube

3 | CONCLUSION

In summary, we have re-investigated the luminescence behavior of the ancient platinocyanides and employed them as model compounds to elucidate the mechanism of unconventional clusteroluminescence phenomenon. Three platinocyanides $BaPt(CN)_4 \cdot 4H_2O$, $K_2Pt(CN)_4 \cdot 3H_2O$, and $Na_2Pt(CN)_4 \cdot 3H_2O$ have been studied and all of them exhibit typical AIE property. Their AIE behaviors have been ascribed to the formation of cluster of $Pt(CN)_4^{2-}$, because the isolated $Pt(CN)_4^{2-}$ is unable to work as a chromophore to emit visible light. Our results indicate that the strong Pt–Pt interactions in the crystal are responsible for the visible emission of these inorganic salts. Furthermore, the rigid 3D network helps suppress the nonradiative decay in the excited state and thus contribute to the high luminescence efficiency. By summarizing the similarities of organic and inorganic clusteroluminescence, we conclude that the enhanced atom–atom/group–group interactions and the rigidification effect after clusterization contribute greatly to the clusteroluminescence phenomenon. Finally, some of these platinocyanides could be excited by X-ray to exhibit RL, which potentially could be used for bioimaging with the advantage of deep penetration depth. This work not only affords a series of inorganic salt-based AIE systems, but also fundamentally helps in understanding both the unconventional organic and inorganic clusteroluminescence phenomena.

ACKNOWLEDGMENTS

The authors are grateful for financial support from the National Natural Science Foundation of China (21788102 and 52003228), the Science and Technology Plan of Shenzhen (JCYJ20180306174910791), the Natural Science Foundation of Guangdong Province (2019B121205002), the Research Grants Council of Hong Kong (N_HKUT609/19, 16305518, A-HKUST605/16, and C6009–17G), and the Innovation and Technology Commission (ITC–CNERC14SC01 and ITCPD/17–9).

FUNDING INFORMATION

National Natural Science Foundation of China, Grant Numbers: 21788102 and 52003228; Science and Technology Plan of Shenzhen, Grant Number: JCYJ20180306174910791; Natural Science Foundation of Guangdong Province, Grant Number: 2019B121205002; Research Grants Council of Hong Kong, Grant Numbers: N_HKUT609/19, 16305518, A-HKUST605/16, and C6009–17G; Innovation and Technology Commission, Grant Numbers: ITC–CNERC14SC01 and ITCPD/17–9

DATA AVAILABILITY STATEMENT

The data that support the findings of this study are openly available in chemrxiv at http://doi.org/10.26434/chemrxiv.8796098.v2

REFERENCES

1. N. A. Spaldin, *Cornell University* **2017**, Accessed: 10th Feb, 2021, https://arxiv.org/abs/1708.01325
2. I. M. Ross, *Bell Labs Tech J* **1997**, *2*, 3
3. M. Lastusaari, T. Laamanen, M. Malkamäki, K. O. Eskola, A. Kotlov, S. Carlson, E. Welter, H. F. Brito, M. Bettinelli, H. Jungner, J. Hölsä, *Eur J Mineral* **2012**, *24*, 885.
4. B. Valeur, M. N. Berberan-Santos, *J Chem Educ* **2011**, *88*, 731.
5. Z. Li, Y. Zhang, X. Wu, L. Huang, D. Li, W. Fan, G. Han, *J Am Chem Soc* **2015**, *137*, 5304.
6. Z. Zhao, H. Zhang, J. W. Y. Lam, B. Z. Tang, *Angew Chem Inter Ed* **2020**, *59*, 9888.
7. H. Zhang, Z. Zhao, A. T. Turley, L. Wang, P. R. McGonigal, Y. Tu, Y. Li, Z. Wang, R. T. K. Kwok, J. W. Y. Lam, B. Z. Tang, *Adv Mater* **2020**, *32*, 2001457.
8. C. Feldmann, T. Jüstel, C. R. Ronda, P. J. Schmidt, *Adv Funct Mater* **2003**, *13*, 511.
9. A. F. van Driel, G. Allan, C. Delerue, P. Lodahl, W. L. Vos, D. Vanmaekelbergh, *Phys Rev Lett* **2005**, *95*, 236804.
10. V. C. -H. Wong, C. Po, S. Y. -L. Leung, A. K. -W. Chan, S. Yang, B. Zhu, X. Cui, V. W. W. Yam, *J Am Chem Soc* **2018**, *140*, 657.
11. Z. Wu, Q. Yao, O. J. H. Chai, N. Ding, W. Xu, S. Zang, J. Xie, *Angew Chem Inter Ed* **2020**, *59*, 9934.
12. X. Jia, X. Yang, J. Li, D. Li, E. Wang, *Chem Commun* **2014**, *50*, 237.
13. Y. Jin, S. Li, Z. Han, B. J. Yan, H. Y. Li, X. Y. Dong, S. Q. Zang, *Angew Chem Int Ed* **2019**, *58*, 12143.
14. J. Shen, Z. Wang, C. Xia, D. Sun, S. Yuan, X. Xin, *Chem Eur J* **2019**, *25*, 4713.
15. Z. Xie, P. Sun, Z. Wang, H. Li, L. Yu, D. Sun, M. Chen, Y. Bi, X. Xin, J. Hao, *Angew Chem Int Ed* **2020**, *59*, 9922.
16. J. Shen, Z. Wang, D. Sun, G. Liu, S. Yuan, M. Kurmoob, X. Xin, *Nanoscale* **2017**, *9*, 19191.
17. P. Sun, Z. Wang, Y. Bi, D. Sun, T. Zhao, F. Zhao, W. Wang, X. Xin, *ACS Appl Nano Mater* **2020**, *3*, 2038.
18. A. Jablonski, *Nature* **1933**, *131*, 839.
19. J. Zhao, S. Ji, Y. Chen, H. Guo, P. Yang, *Phys Chem Chem Phys* **2012**, *14*, 8803.
20. Z. R. Grabowski, K. Rotkiewicz, W. Rettig, *Chem Rev* **2003**, *103*, 3899.
21. Z. Zhao, X. Zheng, L. Du, Y. Xiong, W. He, X. Gao, C. Li, Y. Liu, B. Xu, J. Zhang, F. Song, Y. Yu, X. Zhao, Y. Cai, X. He, R. T. K. Kwok, J. W. Y. Lam, X. Huang, D. Lee Phillips, H. Wang, B. Z. Tang, *Nat Commun* **2019**, *10*, 2952.
22. B. Liu, B. Z. Tang, *Angew Chem Int Ed* **2020**, *59*, 9788.
23. Y. Tu, Z. Zhao, J. W. Y. Lam, B. Z. Tang, *Nat Sci Rev* **2020**. https://doi.org/10.1093/nsr/nwaa260
24. D. Oelkrug, A. Tompert, J. Gierschner, H. -J. Egelhaaf, M. Hanack, M. Hohloch, E. Steinhuber, *J Phys Chem B* **1998**, *102*, 1902.
25. F. Würthner, *Angew Chem Int Ed* **2020**, *59*, 14192.
26. G. Scheibe, *Angew Chem* **1936**, *49*, 563.
27. D. Mobius, *Adv Mater* **1995**, *7*, 437.
28. H. Zhang, Z. Zhao, P. R. McGonigal, R. Ye, S. Liu, J. W. Y. Lam, R. T. K. Kwok, W. Z. Yuan, J. Xie, A. L. Rogach, B. Z. Tang, *Mater Today* **2020**, *32*, 275.
29. H. Wang, Z. Wang, Y. Xiong, S. V. Kershaw, T. Li, Y. Wang, Y. Zhai, A. L. Rogach, *Angew Chem Int Ed* **2019**, *58*, 7040.
30. C. Chen, R. -H. Li, B. -S. Zhu, K. -H. Wang, J. -S. Yao, Y. -C. Yin, M. -M. Yao, H. -B. Yao, S. -H. Yu, *Angew Chem Int Ed* **2018**, *57*, 7106.
31. C. Shang, Y. Zhao, J. Long, Y. Ji, H. Wang, *J Mater Chem C* **2020**, *8*, 1017.
32. X. Chen, T. Yang, J. Lei, X. Liu, Z. Zhao, Z. Xue, W. Li, Y. Zhang, W. Z. Yuan, *J Phys Chem B* **2020**, *124*, 8928.
33. Y. Gong, Y. Tan, J. Mei, Y. Zhang, W. Yuan, Y. Zhang, J. Sun, B. Z. Tang, *Sci China Chem* **2013**, *56*, 1178.
34. J. Galbán, Y. Andreu, J. F. Sierra, S. de Marcos, J. R. Castillo, *Luminescence* **2001**, *16*, 199.
35. A. Pucci, R. Rausa, F. Ciardelli, *Macromol Chem Phys* **2008**, *209*, 900.
36. N. Jiang, D. Zhu, Z. Su, M. R. Bryce, *Mater Chem Front* **2021**, *5*, 60.
37. G. G. Stokes, *Philos Trans R Soc London* **1852**, *142*, 463.
38. J. W. Schindler, R. C. Fukuda, A. W. Adamson, *J Am Chem Soc* **1982**, *104*, 3596.
39. S. B. Piepho, P. N. Schatz, A. J. McCaffrey, *J Am Chem Soc* **1969**, *91*, 5994.
40. C. D. Cowman, H. B. Gray, *Inorg Chem* **1976**, *15*, 2823.
41. A. K. Viswanath. J. Nanosci, *Nanotechnology* **2014**, *14*, 125312.
42. T. Han, C. Gui, J. W. Y. Lam, M. Jiang, N. Xie, R. T. K. Kwok, B. Z. Tang, *Macromolecules* **2017**, *50*, 5807.
43. G. Liang, J. Wu, H. Gao, Q. Wu, J. Lu, F. Zhu, B. Z. Tang, *ACS Macro Lett* **2016**, *5*, 909.
44. X. Zhou, W. Luo, H. Nie, L. Xu, R. Hu, Z. Zhao, A. Qin, B.Z. Tang, *J Mater Chem C* **2017**, *5*, 4775.
45. D. M. Washecheck, S. W. Peterson, A. H. Reis, J. M. Williams, *Inorg Chem* **1976**, *15*, 74.
46. R. L. Maffly, P. L. Johnson, J. M. Williams, *Acta Crystallogr B* **1977**, *33*, 884.
47. P. L. Johnson, T. R. Koch, J. M. Williams, *Acta Crystallogr B* **1977**, *33*, 1976.
48. D. Saito, T. Ogawa, M. Yoshida, J. Takayama, S. Hiura, A. Murayama, A. Kobayashi, M. Kato, *Angew Chem Int Ed* **2020**, *59*, 18723.
49. L. Liu, X. Wang, N. Wang, T. Peng, S. Wan. *Angew Chem Int Ed* **2017**, *56*, 9160.
50. P. Day, *J Am Chem Soc* **1975**, *97*, 1588.
51. J. Mei, Y. Hong, J. W. Y. Lam, A. Qin, Y. Tang, B. Z. Tang, *Adv Mater* **2014**, *26*, 5429.
52. W. Sun, L. Luo, Y. Feng, Y. Cai, Y. Zhuang, R. -J. Xie, X. Chen, H. Chen, *Angew Chem Int Ed* **2020**, *59*, 9914.
53. C. Wang, O. Volotskova, K. Lu, M. Ahmad, C. Sun, L. Xing, W. Lin, *J Am Chem Soc* **2014**, *136*, 6171.
54. T. Guo, Y. Lin, W. -J. Zhang, J. -S. Hong, R. -H. Lin, X. -P. Wu, J. Li, C. -H. Lu, H. -H. Yang, *Nanoscale* **2018**, *10*, 1607.
55. N. Yu, L. Huang, Y. Zhou, T. Xue, Z. Chen, G. Han, *Adv Healthcare Mater* **2019**, *8*, 1801132.

SUPPORTING INFORMATION

Additional supporting information may be found online in the Supporting Information section at the end of the article.

How to cite this article: Zhao Z, Wang Z, Tavakoli J, et al. Revisiting an ancient inorganic aggregation-induced emission system: An enlightenment to clusteroluminescence. *Aggregate*. **2021**;*2*:e36. https://doi.org/10.1002/agt2.36